Computational Medical Physics Working Group Workshop II, Sep 30 – Oct 3, 2007
University of Florida (UF), Gainesville, Florida USA on CD-ROM, American Nuclear Society, LaGrange Park, IL (2007)

IMPLEMENTATION OF SALIVARY GLANDS IN THE BODYBUILDER ANTHROPOMORPHIC PHANTOMS

Kenneth A. Van Riper
White Rock Science
P. O. Box 4729, Los Alamos, NM 87544
kvr@rt66.com

James Roberts and Josephine Clorley
Radiation Protection Service
Velindre Cancer Centre, Cardiff CF14 2TL, UK
James.Roberts@velindre-tr.wales.nhs.uk

ABSTRACT

BodyBuilder [1, 2] is a computer program for the generation of human anthropomorphic phantoms of arbitrary age, from infant through adult. The models are based on the Oak Ridge National Laboratory MIRD specifications [3, 4]. Pregnant females [5], at 3, 6, and 9 months into gestation, including fetal detail, are available. The phantom's sex may be chosen, as well as which organs to include in the model. Organ specific options include using a wall plus contents model for some (such as the stomach) or modeling as a single object, and whether to treat bilateral organs (e.g. lungs) as separate cells or a single combined cell. A graphical user interface controls the selections and operation of the program. Output is in the form of input files for the Monte Carlo N-Particle program MCNP [6]; an alternative output file, containing visualization attributes, facilitates imaging of the geometry by the Moritz [7] and Sabrina [8, 9] graphics programs. BodyBuilder can pass the current model to Moritz or Sabrina, starting the program if necessary. This paper describes the modeling of salivary glands as implemented in the BodyBuilder program. Dosimetry calculations utilizing the salivary gland models will be reported elsewhere by some of us (JR and JC).

KEYWORDS: MCNP, BodyBuilder, Moritz, Sabrina, Salivary Glands

1. BODYBUILDER MODELS

The BodyBuilder components are bounded by first and second order surfaces. Fig. 1 is three dimensional (3D) view of the head showing the cranium, jawbone, and spine inside the semi-transparent flesh. The salivary glands are not included. The models are oriented with the Z axis as vertical and the positive Y axis in the posterior direction. From the outside in, the lower part of the head consists of skin, an undifferentiated tissue layer, the jawbone, and more tissue. These layers are bounded, in part, by concentric and congruent elliptical cylinders centered on the Z axis at X = Y = 0. Fig. 2 is a horizontal slice through the head intersecting the jawbone and spine. It shows the elliptical cylinders bounding the various components. The thick outermost cylinder is the skin. The jawbone extends from the mid-plane (Y = 0, blue in Fig. 2) of the head forward.

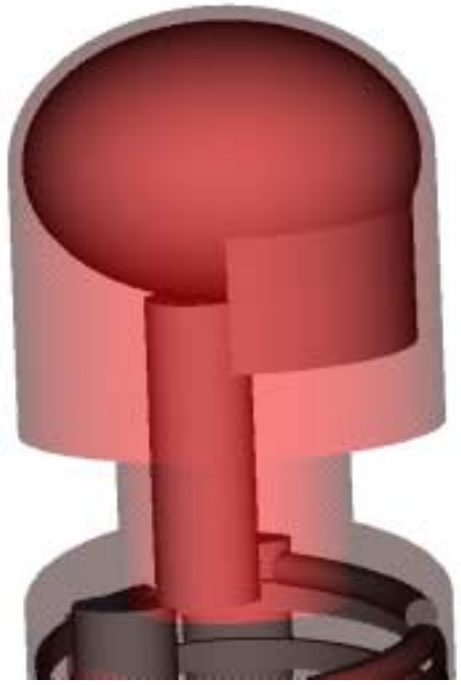

Figure 1. Head showing semi-transparent flesh and bones (solid gray).

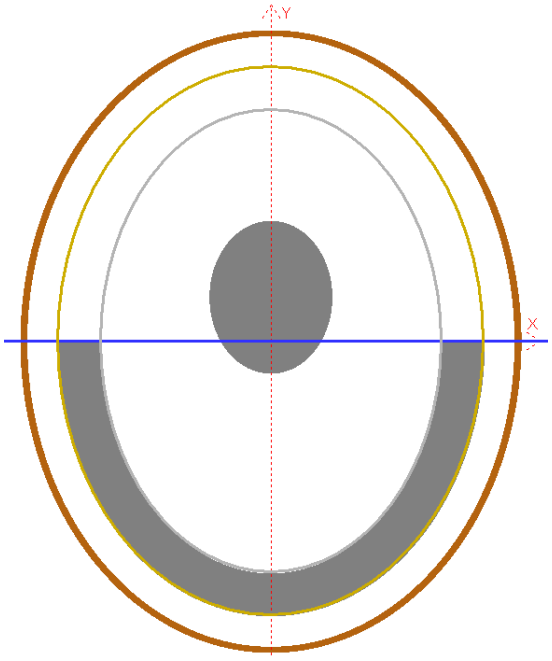

Figure 2. Horizontal slice including the jawbone and spine.

2. SALIVARY GLANDS

We modeled the three main glands: parotid, submandibular, and sublingual. They are present as left/right pairs; each is reflectively symmetric about Y = 0. The user can choose to

treat each of the three glands as separate left and right cells or as a combined left + right cell. In either case, the parotid, submandibular, and sublingual glands are distinct cells. Fig. 3 shows side and rear views of the head including the glands. In the side view, the jawbone and cranium are semi-transparent to reveal the interior glands.

The initial gland descriptions were taken from Moore and Dalley [10]. These have been used to determine the appropriate shape, size and position of the modeled glands. Diagrams and CT images were also used as a compliment to the descriptions. We added several refinements during implementation.

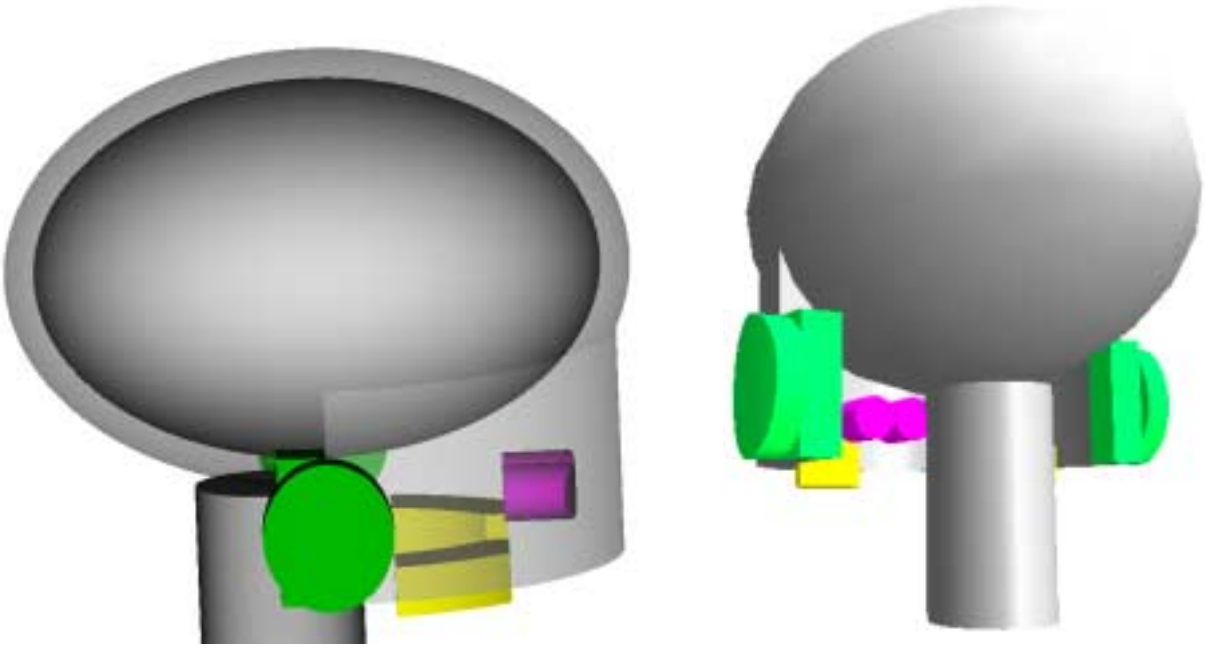

Figure 3. Parotid (green), submandibular (yellow), and sublingual (magenta) glands.

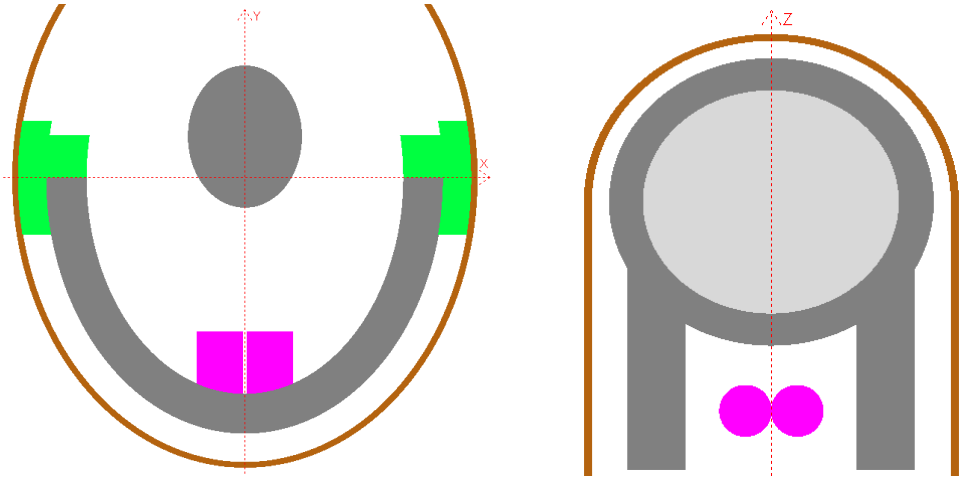

Figure 4. Horizontal (left) and vertical slices (right) through the sublingual glands.

2.1. Sublingual Glands

The sublingual glands (magenta in the figures) are bounded by two cylinders in the Y direction that are tangent at X = 0. The Z value for their centers is the top of the spine. The cylinders are cut off by the inner jawbone surface and a plane perpendicular to the cylinders chosen to give an approximate length of 2 cm. The dimensions cited are for the male adult model before adjustments to match volumes.

Fig. 4 shows two slices intersecting the sublingual glands. In these figures, bones are dark gray, the brain is light gray, and the skin is brown. The arrows show the coordinate directions.

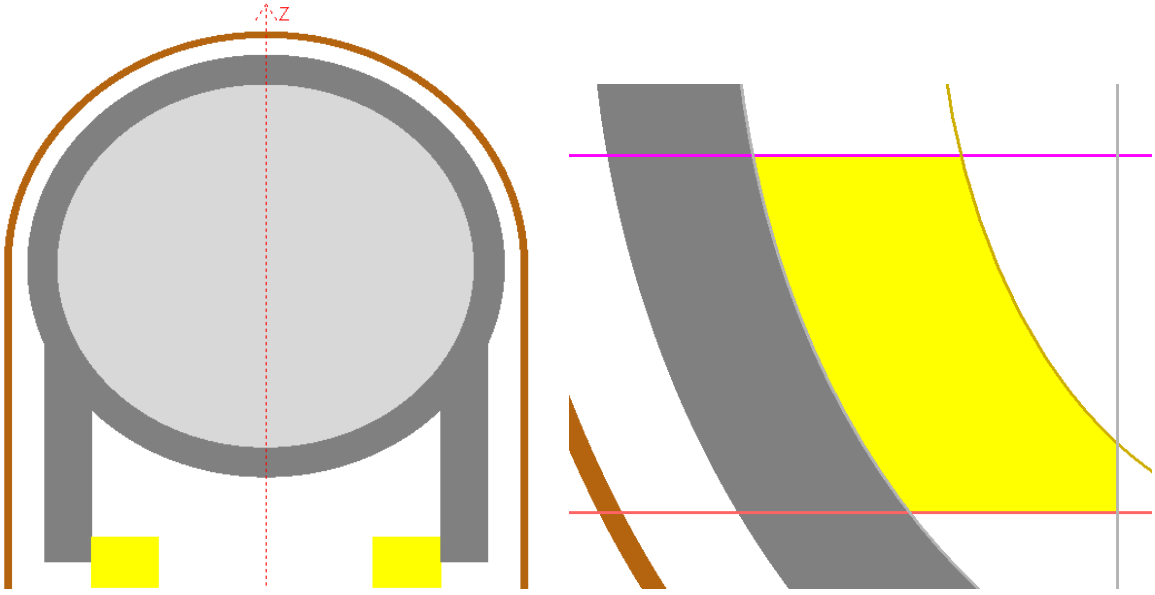

Figure 5. Vertical (left) and horizontal (right) slices through the submandibular glands.

2.2. Submandibular Glands

The submandibular glands (yellow in the figures) are centered in the Z direction on the lower edge of the jawbone and are approximately 2 cm thick in that direction. The left panel of Fig. 5 shows the vertical extent. The other surfaces bounding the submandibular glands are an elliptical cylinder congruent to the elliptical cylinder of the inner jawbone surface but with radii 2 cm smaller and planes at Y = -2 cm, Y = -5.5 cm, and X = ±1.8 cm. The right panel of Fig. 5 shows the bounding surfaces in a horizontal plane.

2.3. Parotid Glands

Each of the parotid glands (green in the figures) consists of two parts. The inner part, visible in the left panel of Fig. 6, lies between the two elliptical cylinders that bound the jawbone. It is bounded in front by the rear edge of the jawbone and in the rear by a plane at Y = 1.5 cm. The bottom is coincident with the lower edge of the jawbone as shown in the right panel of Fig. 6. The height is 4 cm. The outer parts of the parotid glands lie between the elliptical Z cylinders for the inner skin and outer jawbone surfaces and an elliptical cylinder parallel to the X axis. Fig. 7 shows a vertical slice intersecting the outer part. The center of the latter cylinder is 2

cm above the lower edge of the jawbone in the Z direction and at Y = 0. The radii are 2.3 cm (Z direction) and 2 cm (Y direction).

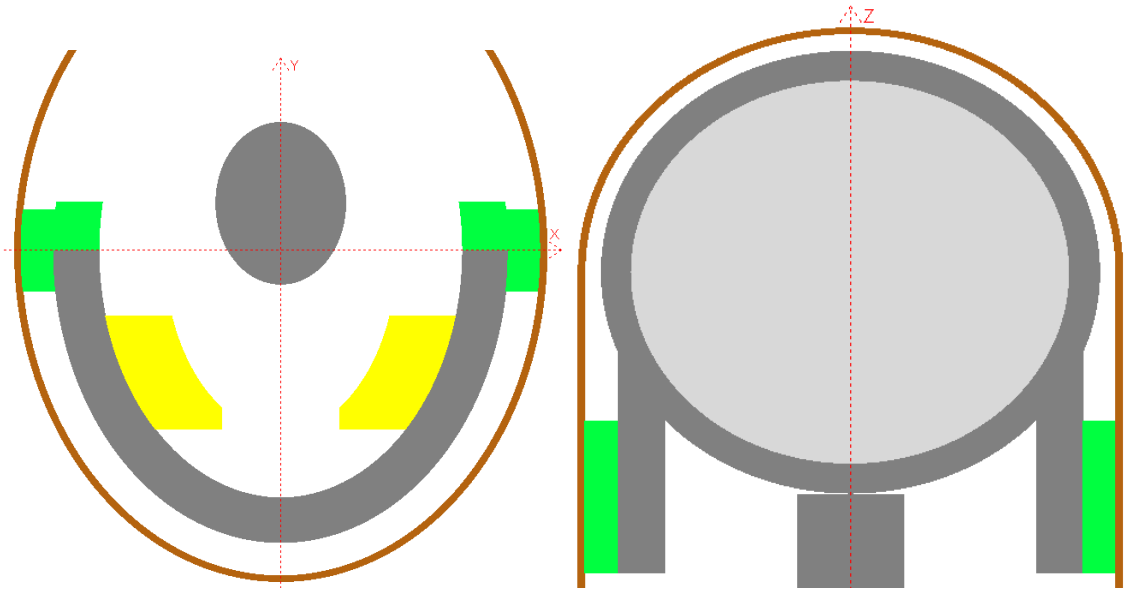

Figure 6. Horizontal (left) and vertical (right) slices through the parotid glands.

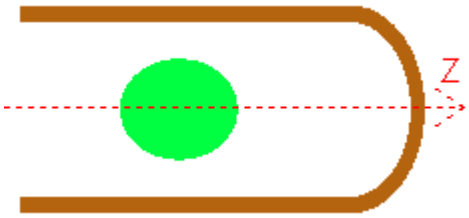

Figure 7. Vertical slice through the outer part of the submandibular glands.

3. GLAND MASSES

We calculated the volumes of the modeled salivary glands using the volume fraction feature of the Moritz program. We then adjusted some of the dimensions to match the volumes given by ICRP 89 [11]. In addition to the adult male, BodyBuilder generates models at ages between 1 year and adult and a newborn model. As a first approximation to accommodate the smaller head sizes of these models, we multiplied the dimensions of the salivary glands by the ratio of the semi-major radius of the outer jawbone elliptical cylinder for the current age to the value of the adult radius. We calculated the volumes and adjusted the dimensions to match ICRP 89 as for the adult model. The volume matching procedure was also performed for the newborn and 1-, 5-, 10-, and 15-year old models (BodyBuilder interpolates between these models for other ages).

4. CONCLUSIONS

We have implemented models of the parotid, submandibular, and sublingual salivary glands in the BodyBuilder program. For each age, the gland masses match those specified by ICRP 89. The salivary glands are a standard BodyBuilder feature as from version 1.31.

Fig. 8 shows additional 3D views of the head including the salivary glands. In the front view on the right, the jawbone and cranium are semi-transparent.

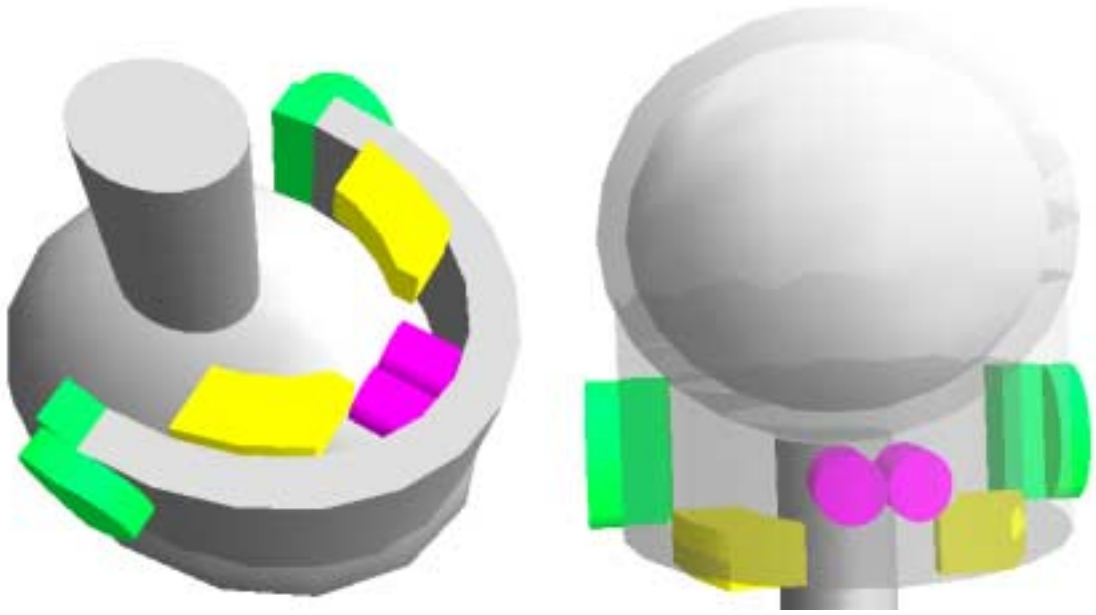

Figure 7. Bottom (left) and front (right) views of the head.

REFERENCES

1. K. A. Van Riper, D. L. Spikes, and R. G. McDowell, 1 *Proceedings of the 1996 Topical Meeting Radiation Protection & Shielding*, No. Falmouth, MA, April 21–25, p 643, (1996).
2. R. H. Olsher and K. A. Van Riper, "Application of a Sitting MIRD Phantom for Effective Dose Calculations", *Radiation Protection Dosimetry*, **116, No. 1–4**, 392–395 (2005).
3. M. Cristy and K. F. Eckerman, *Specific Absorbed Fractions of Energy at Various Ages from Internal Photon Sources, I. Methods*, ORNL/TM-8381/V1, Oak Ridge National Laboratories (1987).
4. K. F. Eckerman, M. Cristy, and J. C. Ryman, *The ORNL Mathematical Phantom Series*, Oak Ridge National Laboratory Report, available at http://homer.hsr.ornl.gov/VLab/VLabPhan.html, (1996)
5. M. G. Stabin, E. E. Watson, M. Cristy, J. C. Ryman, K. F. Eckerman, J. L. Davis, D. Marshall, and M. K. Gehlen, *Mathematical Models and Specific Absorbed Fractions of Photon Energy in the Nonpregnant Adult Female and at the End of Each Trimester of Pregnancy*, Oak Ridge National Laboratory Report ORNL/TM-12907, (1995).

6. J. F. Briesmeister, Editor, *MCNP – A General Monte Carlo N-Particle Transport Code*, Los Alamos National Laboratory Report LA-13709-M, (2000).
7. K.A. Van Riper, "Interactive 3D Display of MCNP Geometry Models," *Proceedings of the ANS International Meeting on Mathematical Methods for Nuclear Applications*, Salt Lake, UT, Sept. 10–13, (2001).
8. J.T. West III, *SABRINA: An Interactive Three-Dimensional Geometry-Modeling Program for MCNP*, Los Alamos National Laboratory Report LA–10688–M (1986).
9. K.A. Van Riper, "New Features in Sabrina," *Proceedings of the Topical Meeting on Radiation Protection for our National Priorities*, Spokane, WA, Sept. 17–21, 2000, pp. 316–323 (2000).
10. K. L. Moore, and A. F. Dalley, *Clinically Orientated Anatomy, 4th edition*, Lippingcott Williams & Wilkins.
11. The International Commission on Radiological Protection (ICRP), Annals of the ICRP – Publication 89, *Basic Anatomical and Physiological Data for Use in Radiological Protection: Reference Values*, (2002).